

Increased crevassing across accelerating Greenland Ice Sheet margins

Thomas R. Chudley

Department of Geography, Durham University, Durham, UK

<https://orcid.org/0000-0001-8547-1132>

Ian M. Howat

Byrd Polar and Climate Research Center, Ohio State University, Columbus, OH, USA

School of Earth Sciences, Ohio State University, Columbus, OH, USA

<https://orcid.org/0000-0002-8072-6260>

Michalea D. King

Polar Science Center, University of Washington, Seattle, WA, USA

<https://orcid.org/0000-0002-8138-4362>

Emma J. MacKie

Department of Geological Sciences, University of Florida, Gainesville, FL, USA

<https://orcid.org/0000-0002-6303-5249>

Correspondence: Tom Chudley (thomas.r.chudley@durham.ac.uk)

Increased crevassing across accelerating Greenland Ice Sheet margins

Thomas R. Chudley^{1,2}, Ian M. Howat^{2,3}, Michalea D. King⁴, Emma J. MacKie⁵

5 ¹ Department of Geography, Durham University, Durham, UK

² Byrd Polar and Climate Research Center, Ohio State University, OH, USA

³ School of Earth Sciences, Ohio State University, OH, USA

⁴ Polar Science Center, University of Washington, WA, USA

⁵ Department of Geological Sciences, University of Florida, FL, USA

10

Correspondence: Tom Chudley (thomas.r.chudley@durham.ac.uk)

Abstract

The extent of surface crevassing on the Greenland Ice Sheet is a large source of
uncertainty in processes controlling mass loss, including iceberg calving, ice rheology, and
15 water routing. However, no work to date has comprehensively mapped the location of
surface crevasses or examined their evolution through time. Here, we use high-resolution
digital elevation models to map the 3-dimensional volume of crevasse fields across the
Greenland Ice Sheet in 2016 and 2021. Whilst the change in the total volume of crevasses
between these two years was within measurement error ($+4.3 \pm 5.9\%$), large and
20 significant increases occurred at accelerating marine-terminating sectors of the ice sheet
(up to $+25.3 \pm 10.1\%$). These increases were offset only by a reduction in crevasse
volume in the central west sector ($-14.2 \pm 3.2\%$), particularly at Sermeq Kujalleq
(Jakobshavn Isbræ), which underwent a temporary slowdown over the study period.
Changes in crevasse volume correlate strongly with antecedent discharge changes,
25 indicating that Greenland's acceleration is affecting significant increases in crevassing on
a timescale of less than five years. This rapid response provides a mechanism for mass-
loss-promoting feedbacks on sub-decadal timescales, including increased calving, faster
flow, and accelerated water transfer to the bed.

Main

30 Surface crevasses result from spatial and temporal ice flow variability and, thus, are
ubiquitous across the complex, fast-flowing margins of the Greenland Ice Sheet (GrIS).
Crevasses exert a first-order control on varied glaciological processes: fractures can act as

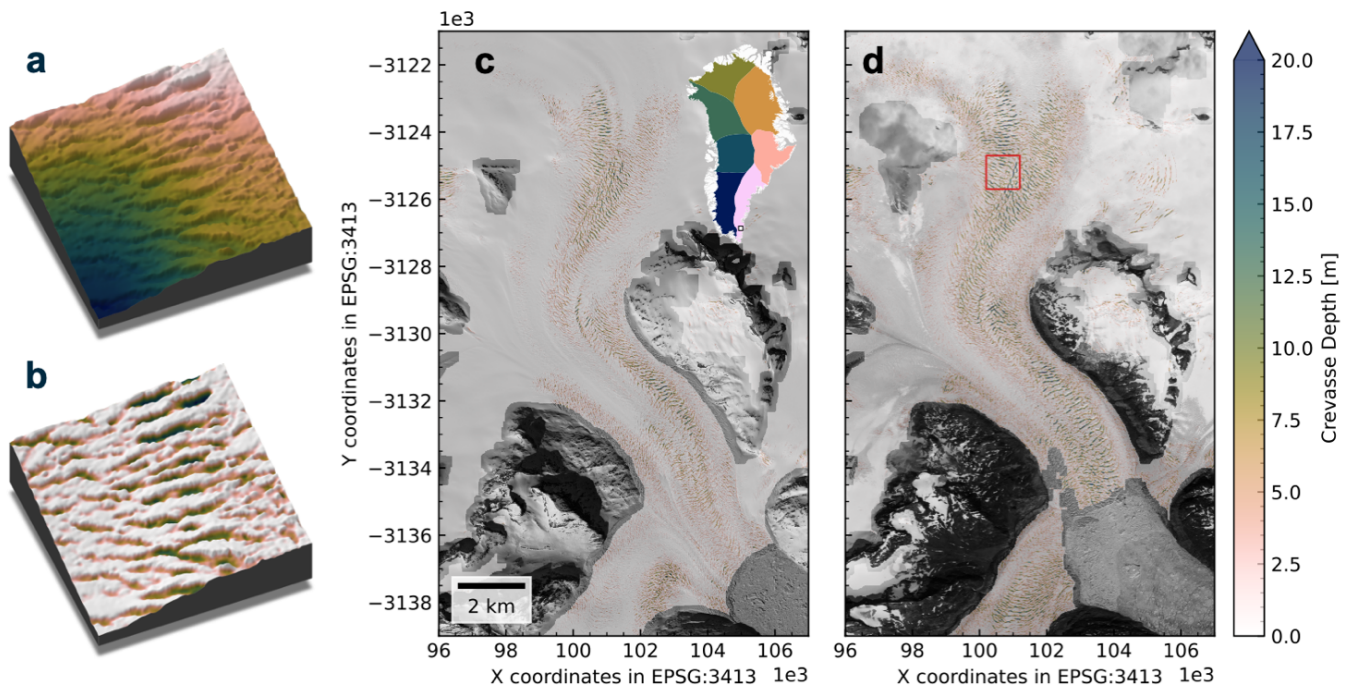
pre-existing weaknesses that can promote calving and instability at glacier fronts ¹, whilst accumulated damage can soften the large-scale rheology of ice ². As key hydrological pathways ³⁻⁵, crevasses transfer up to half of Greenland's seasonal surface runoff to the bed ⁶. This transport can alter ice rheology by increasing ice temperature ⁷, modify the pressure of the subglacial hydrological system ^{4,5,8,9}, and promote basal melt ¹⁰. By modulating the rate of meltwater transport to the ocean, further influence is exerted on terminus melt, fjord circulation, and fjord biogeochemistry ¹¹⁻¹³. These crevasse-dependent processes hold the potential to induce significant feedbacks between ice flow acceleration and mass loss ^{4,14}, making them a key source of uncertainty in projections of future Greenland Ice Sheet behaviour ^{1,15}.

Given these mass-loss-accelerating feedbacks, it is critical to understand how crevasse fields are changing across Greenland. It is expected that increases in crevasse extent are common across the ice sheet due to a (i) increasing tensile stresses resulting from a steepening ablation area and outlet glacier acceleration ¹⁴, and (ii) an increase in meltwater available for hydrofracture ⁹. Only one multitemporal study exists, which observed an increase crevasse extent across a region of West Greenland between 1985 and 2009 ⁴. However, observations of surging glaciers have shown that crevasse fields can propagate on much faster timescales (months - years) in response to rapid dynamic change ^{16,17}. Outlet glaciers around the GrIS are exhibiting accelerations of the same magnitude and rate as glacier surges ¹⁸⁻²⁰, suggesting that recent accelerations could initiate crevasse growth and subsequent feedbacks over sub-decadal timescales. However, no study has yet monitored short-term change in crevassing in Greenland, nor conducted a comprehensive assessment across the full ice sheet.

Recognition of crevassing's importance has motivated improved observation and modelling capabilities. Studies have shown that simple parameterisations used in modelling studies are not a good predictor of crevasse distribution ^{3,21} due to mixed-mode fracture formation ²², variable ice rheology ²³, and the advection of crevasses from zones of active opening ²⁴. Therefore, improved observations are required to develop and validate models of fracture formation and propagation ²⁵ and parameterise their behaviour in models of ice sheet dynamics and hydrology ^{6,26}. Optical satellite observation methods have progressed from manual delineation ⁴ to computer vision ^{27,28} and machine learning ^{29,30} approaches. However, these are limited to assessing crevasse presence without critical information about crevasse depth, and attempts to map geometry have thus far been limited to profiles ²¹. Recent public availability of comprehensive, multitemporal, and high-resolution digital elevation models (DEMs) of the polar regions ³¹ provide an

70 unprecedented opportunity to assess 3-D crevasse geometry and evolution at high spatial
and temporal resolution. Here, we use these data to present the first three-dimensional
record of crevassing over the entire GrIS from 2016 to 2021, a period of time with
significant dynamic accelerations^{18–20} and decelerations³². We use these maps to
75 quantify the rate and extent of regional trends in crevassing and provide the first ice-sheet-
wide observational evidence of the relationship between crevassing and ice dynamic
change.

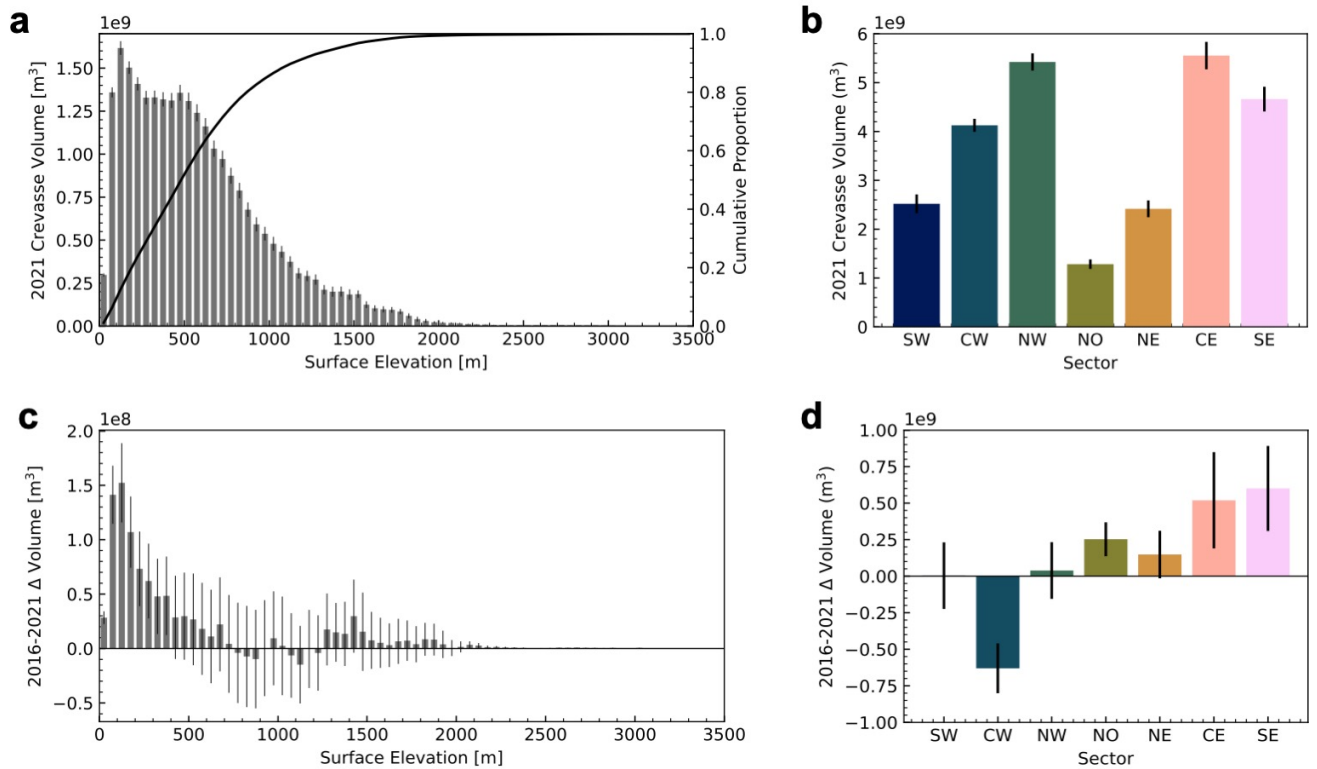
Multitemporal Greenland-wide crevasse inventories



80

Figure 1: Examples of crevasse field extraction and evolution from ArcticDEM

strips. (a) A 500×500 m ArcticDEM sample of a crevassed surface. (b) Sample following
crevasse extraction, with a colour scale matching panels c and d. (c) Crevasse depths at
the head of Anorituup Kangerlua fjord from a 2016-04-13 ArcticDEM strip, overlaid onto a
85 contemporaneous Worldview-1 image. (d) Same as (c), but for 2021-07-15 after sustained
acceleration and retreat. Red box identifies regions of panels a and b. Inset: location of
Anorituup Kangerlua fjord (white box) within Greenland, with sectors in Figs. 2 and 3
coloured separately.



90

Figure 2: Crevasse volume and changes across the ice sheet. (a) Histogram of 2021 crevasse volume with surface elevation across the ice sheet. (b) Bar chart of 2021 crevasse volume per sector. (c) Histogram of 2016-2021 crevasse volume change with surface elevation across the ice sheet. (d) Bar chart of 2016-2021 crevasse volume change per sector. Error bars represent 2σ measurement uncertainties (see methods).

95

We extracted crevasse depth from 2 m resolution ArcticDEM strips³¹ across the GrIS in 2016 and 2021 (Fig. 1; Methods). We integrated pixel-based crevasse depth to estimate the air-filled crevasse volume, providing the first estimates of crevasse inventory and change at an ice sheet, sector, and basin scale.

100

In 2021, we mapped an estimated $25.98 \times 10^9 \pm 1.30 \times 10^9 \text{ m}^3$ of crevasse volume across $\sim 89\%$ of the melt zone (see Methods) of the GrIS. Crevasse distribution overwhelmingly dominated low elevations near the ice margin (Fig. 2a), with 68% of crevasse volume concentrated below 700 m above mean sea level (AMSL), and 95% below 1420 m AMSL. However, crevasses were less present at the lowest elevations, below 100 m AMSL (Fig. 2a), mostly due to the height of marine-terminating ice cliffs³³.

105

Hence, beneath 100 m ice either does not exist (it has already calved) or is land-terminating without significant crevassing. Significant sectoral variation was observed (Fig. 2b), with high volumes of crevasses in the CE, NW, SE, and CW sectors (typified by large, fast-flowing, marine outlets), and lower volumes in the land-terminating SW and less-dynamic NO and NE sectors. The crevasse elevation distribution was also highly variable

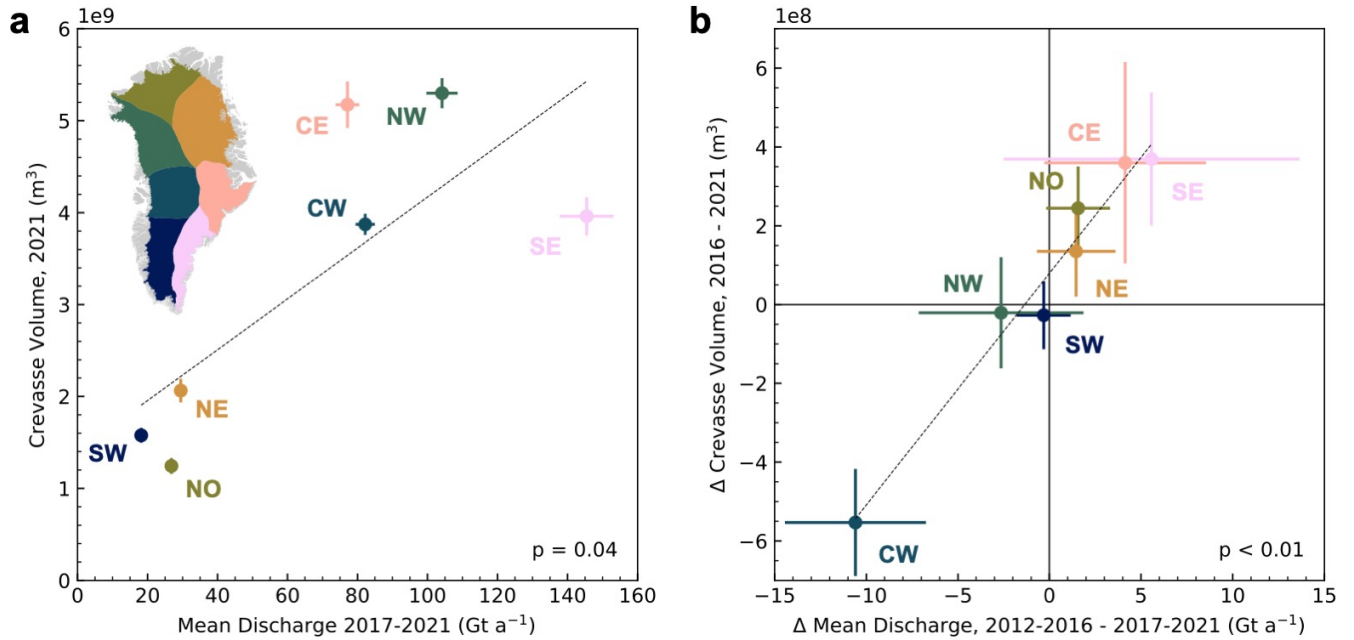
110

115 between sectors (Extended Data Fig. 1). Sector NW exhibited a sharp elevation gradient in crevasse volumes, up to 1000 m AMSL, whilst the similarly marine-terminating SE and CE sectors had longer-tailed distributions up to 2000 m AMSL. This reflects the typical long
120 trunks of SE/CE sectors, which extended diffusive acceleration from the ice front along their length, whilst NW glaciers are closely linked to the surrounding ice sheet with strongly convergent flow until close to the glacier margins^{34,35}. Sector NO and NE are characterised by a low-elevation bias, with little crevassing above 150 m. This likely
125 reflects the predominance of crevassing on floating ice tongues concentrated in these sectors³⁶. Finally, the unique distribution of sector CW, with the bulk of crevassing between the 200-800 m AMSL elevation bands, reflects the dominance of large marine-terminating outlets with short trunks and high calving fronts such as Sermeq Kujalleq (Jakobshavn Isbræ) (hereafter SKJI).

130 The change in crevasse volume from 2016 and 2021 across the Greenland Ice Sheet was within measurement uncertainty, with a total change in crevasse volume of $+9.32 \times 10^8 \pm 13.01 \times 10^8 \text{ m}^3$ ($+4.3 \pm 5.9\%$). However, this total masks spatially heterogeneous behaviour by elevation and sector. Beneath 400 m AMSL, crevasse volume increased
135 significantly across all elevations, peaking at 100-150 m AMSL (Fig. 2c). Beneath ~100 m AMSL, increased crevassing was offset by a loss of surface area as marine-terminating glaciers retreated. Changes were highly heterogeneous at a sectoral level (Fig. 2d), varying between $+25.3 \pm 10.1\%$ (NO) to $-14.2 \pm -3.2\%$ (CW). No significant changes were observed in the NW or NE, nor the land-terminating SW, whilst significant increases in the
140 NO, CE, and SE were offset by a large reduction in the volume of crevasses in the CW sector (fig. b). Sectors displayed distinct elevation distributions (Extended Data Fig. 2). In the NO and NE, increases were limited to ice tongues at the lowest elevations ($< \sim 400$ m AMSL), whilst increases in the CE and SE were distributed more evenly across the lowest ~1000 m AMSL due to diffusive thinning along the trunk.

140 **Relationship to dynamics**

Changes in crevasse morphology and extent reflect changes in ice dynamics: specifically, the surface stress regime^{1,37,38}. We used records of total ice flux through outlet glacier termini, termed discharge, as a proxy for the bulk dynamic change of ice sectors and basins. This proposed relationship between discharge and crevasse volume holds at a
145 sectoral scale in our dataset (Fig. 3a; $p = 0.04$). Sectors with high proportions of slow-flowing, land-terminating margins (SW), or less dynamic, well-buttressed outlet glaciers (NO/NE) exhibited low crevasse volumes compared to sectors with high numbers of fast-flowing marine-terminating outlets (SE/CE/NW/CW).



150

Figure 3: Sectoral-scale discharge comparison. (a) Scatter plot showing sectoral-scale relationships between 2017-2021 mean annual discharge and 2021 crevasse volume. Error bars represent 2σ uncertainties. (b) Scatter plot showing sectoral-scale relationship between change in mean annual discharge between the 2011-2016 and 2017-2021 periods and change in crevasse volume between 2016-2021. Error bars represent 2σ uncertainties. Note that only drainage basins with $>60\%$ crevasse observations and valid discharge records are included in the sectoral sum totals. Full regression results are presented in Supplementary Table 1.

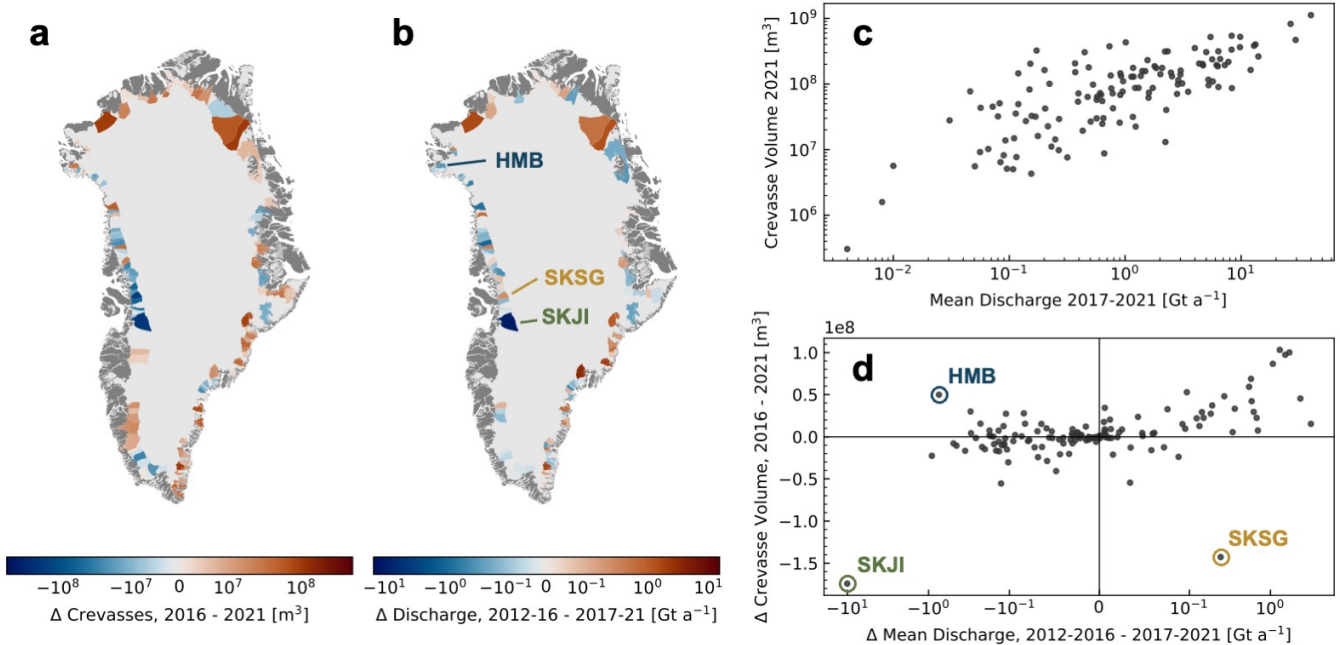
160

We found a striking, sector-scale relationship (fig. 3b; $p < 0.01$) between the change in crevasse volumes between 2016-2021 and the change in the antecedent five-year mean discharge (between 2012-2016 and 2017-2021; see Methods), consistent with the hypothesis that changes in crevasse volume and extent are forced by changes in the dynamic regime of glaciers. Reductions in discharge from the CW sector in the second half of the 2010s are well documented³⁹, largely driven by SKJI, which has exhibited significant slowdown since 2014 following a reduction in ocean forcing^{32,40}. Meanwhile, increased crevassing across the CE and SE sectors were consistent with accelerating ice velocities and discharge observed at both glacier and sectoral levels, linked to warming air and ocean temperatures^{18,19,41,42}.

170

We further assessed crevasse volume and changes at a basin level (Fig. 4a-b). This analysis confirmed a significant positive relationship ($p < 0.01$) between discharge and

175 crevasse volume (Fig. 4c). This relationship exhibits a higher variability than the sectoral scale. We suggest that this relationship is analogous to the Greenland discharge literature, whereby large-scale forcing is modulated by glacier-specific factors including, among
 180 others, fjord and glacier geometry⁴³. In our case, local factors modulating the relationship between discharge and crevasse expression may include ice rheology (ice temperature, pre-existing damage, etc), the specific distribution of stresses (e.g. plug flow concentrating high surface stresses into shear margins), and other factors including ice velocity, thickness, and basal traction.



185 **Figure 4: Basin-scale discharge comparison.** (a) Change in crevasse volume between 2016-2021 at a basins with significant (>60%) map coverage. (b) Change in mean annual discharge between the 2011-2016 and 2017-2021 periods. (c) Basin-scale relationship between 2017-2021 mean annual discharge and 2021 crevasse volume. (d) Basin-scale relationship between change in mean annual discharge between the 2011-2016 and 2017-2021 periods and change in crevasse volume between 2016-2021. Outliers Harald Moltke
 190 Bræ (HMB), Sermeq Kujalleq (Jakobshavn Isbræ; SKJI), and Sermeq Kujalleq (Store Glacier; SKSG) are labelled. Only basins of a total area > 100 km² are shown.

195 More nuance is revealed in the relationship between change in discharge and change in crevassing (Fig. 4d). Although there was a significant relationship between an increase in discharge and an increase in crevassing ($p < 0.01$ where Δ discharge > 0), there appeared to be a weaker relationship between crevassing and a decrease in discharge: in fact, the only glacier to display a significant reduction in both discharge and crevassing was SKJI. After excluding SKJI, the relationship was not significant ($p = 0.44$ where Δ discharge < 0).

200 We suggest this could relate to differing timescales required to open and close crevasse
fields, consistent with previous work that has concluded that crevasse formation outpaces
crevasses closure^{37,44}. Opening of crevasse fields likely occurs rapidly (< five years),
forced by the higher tensile surface stresses occurring alongside ice acceleration.
However, an equivalent reduction in velocity at outlet glaciers does not necessitate a
compressive stress regime that would actively close crevasses. Instead, the closure of
205 crevasse fields requires the generational replacement of individual crevasses within a field
by smaller crevasses formed under lower-tensile-stress conditions. As such, any reduction
in crevasse field volume is rate-limited by surface velocity. The reduction in crevasse
volume shown here at SKJI (labelled in Fig. 4d) may be an instructive exception,
demonstrating how the fast-flowing regime propagated crevasse closure within a five-year
210 timescale. Alternatively, the rapid collapse in velocities at SKJI after 2016³² could have
induced a sufficiently large regions of compression to actively close crevasses on a short
timescale.

Further individual basin-level anomalies also provide insights into crevasse behaviours.
215 For instance, Harald Moltke Bræ (HMB in Fig. 4d) showed distinct reduction in discharge
yet an increase in crevassing. This was an aliasing effect related to the surge occurring
2013-2019⁴⁵, which resulted in an increase in (relict) crevasses between 2016 and 2021
even as the discharge reduced. Sermeq Kujalleq (Store Glacier) (SKSG hereafter and in
Fig. 4d) exhibits the opposite anomaly, undergoing significant decreases in crevasse
220 volume despite an increase in discharge. We hypothesise that this may relate to rapid
summer deceleration events that occurred in 2018 and 2019 (Supplementary Fig. 1).
SKSG consistently displays these behaviours, likely associated with instabilities in basal
hydrology and sliding. However, the deceleration events in these two summers were
particularly extreme, with velocity collapsing by as much as 50% in 2019 (Supplementary
225 Fig. 2). The resulting perturbation to the glacier strain field may have contributed to a
reduced crevasse volume. If these seasonal deceleration events were contributory factors,
the magnitude and variability of deceleration events may have an outsized impact on
crevasse evolution in glaciers that exhibit this behaviour.

Implications

230 We provide the first, Greenland-wide observations of crevasse volume and distribution,
revealing significant changes in crevassing from 2016 to 2021 (sectoral-scale variation
from -14.2% to +25.3%) that correlate with the dynamic evolution of marine-terminating
outlets. Although total change ($+4.3 \pm 5.9\%$) is within measurement uncertainty, significant
sector-scale increases in crevassing occur in most sectors (Fig. 2d), offset by only a few

235 glaciers in the CW sector – in particular SKJI, which is known to have undergone a
significant slowdown between 2016-2019³². Recent data indicate that SKJI is once again
exhibiting acceleration and associated dynamic thinning⁴⁸, suggesting that SKJI will no
longer offset Greenland-wide increases in crevassing in the near future. The five-year
240 timescale assessed here provides evidence of crevasse response time to dynamic
changes in Greenland an order-of-magnitude faster than previously identified by satellite
observation⁴.

The ability to observe crevasses in 3-D provides a major advance over two-dimensional
mapping from imagery alone^{27,28}. We have observed significant increases in crevasse
245 volume in pre-existing crevasse fields at low elevations (marine-terminating outlets). This
change, not previously able to be assessed, highlights a pathway for externally forced
(ocean- or atmosphere-driven) dynamic accelerations to generate a number of positive
feedbacks to ice loss to through increased crevassing³⁷. Increased damage over annual
timescales can act to weaken shear margins². By transferring water to the bed^{4,6,26},
250 crevasses induce rheological changes^{7,14}, modify basal friction⁴, and – upon reaching the
ocean – amplify submarine melting at the terminus¹³. Finally, crevasses advected to the
calving front play a role in accelerating glacier calving^{1,49}. The ice-sheet-wide methods,
datasets, and behaviours presented here provide a starting point to properly calibrate and
validate damage representation in large-scale dynamic models, accommodating the
255 effects of ice damage and crevassing into predictions of future ice sheet behaviour.

References

1. Berg, B. & Bassis, J. Crevasse advection increases glacier calving. *Journal of Glaciology* **68**, 977–986 (2022).
2. Lhermitte, S. *et al.* Damage accelerates ice shelf instability and mass loss in
260 Amundsen Sea Embayment. *Proceedings of the National Academy of Sciences* **117**,
24735–24741 (2020).
3. Chudley, T. R. *et al.* Controls on Water Storage and Drainage in Crevasses on the
Greenland Ice Sheet. *Journal of Geophysical Research: Earth Surface* **126**,
e2021JF006287 (2021).
- 265 4. Colgan, W. *et al.* An increase in crevasse extent, West Greenland: Hydrologic
implications. *Geophysical Research Letters* **38**, (2011).
5. McGrath, D., Colgan, W., Steffen, K., Lauffenburger, P. & Balog, J. Assessing the
summer water budget of a moulin basin in the Sermeq Avannarleq ablation region,
Greenland ice sheet. *Journal of Glaciology* **57**, 954–964 (2011).

- 270 6. Koziol, C., Arnold, N., Pope, A. & Colgan, W. Quantifying supraglacial meltwater pathways in the Paakitsoq region, West Greenland. *Journal of Glaciology* 1–13 (2017) doi:10.1017/jog.2017.5.
7. Lüthi, M. P. *et al.* Heat sources within the Greenland Ice Sheet: dissipation, temperate paleo-firn and cryo-hydrologic warming. *The Cryosphere* (2015) doi:10.5194/tc-9-245-275-2015.
8. Cavanagh, J. P., Lampkin, D. J. & Moon, T. Seasonal Variability in Regional Ice Flow Due to Meltwater Injection Into the Shear Margins of Jakobshavn Isbræ. *Journal of Geophysical Research: Earth Surface* **122**, 2488–2505 (2017).
9. Lampkin, D. J., Amador, N., Parizek, B. R., Farness, K. & Jezek, K. Drainage from water-filled crevasses along the margins of Jakobshavn Isbræ: A potential catalyst for catchment expansion. *Journal of Geophysical Research: Earth Surface* **118**, 795–813 (2013).
- 280 10. Young, T. J. *et al.* Rapid basal melting of the Greenland Ice Sheet from surface meltwater drainage. *Proceedings of the National Academy of Sciences* **119**, e2116036119 (2022).
- 285 11. Cowton, T., Slater, D., Sole, A., Goldberg, D. & Nienow, P. Modeling the impact of glacial runoff on fjord circulation and submarine melt rate using a new subgrid-scale parameterization for glacial plumes. *Journal of Geophysical Research: Oceans* **120**, 796–812 (2015).
- 290 12. Kanna, N. *et al.* Meltwater Discharge From Marine-Terminating Glaciers Drives Biogeochemical Conditions in a Greenlandic Fjord. *Global Biogeochemical Cycles* **36**, e2022GB007411 (2022).
13. Slater, D. A. & Straneo, F. Submarine melting of glaciers in Greenland amplified by atmospheric warming. *Nat. Geosci.* 1–6 (2022) doi:10.1038/s41561-022-01035-9.
- 295 14. Colgan, W., Sommers, A., Rajaram, H., Abdalati, W. & Frahm, J. Considering thermal-viscous collapse of the Greenland ice sheet. *Earth's Future* **3**, 252–267 (2015).
15. Alley, R. B. *et al.* Iceberg Calving: Regimes and Transitions. *Annual Review of Earth and Planetary Sciences* **51**, 189–215 (2023).
16. Herzfeld, U. C. & Mayer, H. Surge of Bering Glacier and Bagley Ice Field, Alaska: an update to August 1995 and an interpretation of brittle-deformation patterns. *Journal of Glaciology* **43**, 427–434 (1997).
- 300 17. Trantow, T. & Herzfeld, U. C. Crevasses as Indicators of Surge Dynamics in the Bering Bagley Glacier System, Alaska: Numerical Experiments and Comparison to Image Data Analysis. *Journal of Geophysical Research: Earth Surface* **123**, 1615–1637 (2018).
- 305

18. Bevan, S. L., Luckman, A. J., Benn, D. I., Cowton, T. & Todd, J. Impact of warming shelf waters on ice mélange and terminus retreat at a large SE Greenland glacier. *The Cryosphere* **13**, 2303–2315 (2019).
19. Chudley, T. R., Howat, I. M., King, M. D. & Negrete, A. Atlantic water intrusion triggers rapid retreat and regime change at previously stable Greenland glacier. *Nat Commun* **14**, 2151 (2023).
20. Williams, J. J., Gourmelen, N. & Nienow, P. Complex multi-decadal ice dynamical change inland of marine-terminating glaciers on the Greenland Ice Sheet. *Journal of Glaciology* 1–14 (2021) doi:10.1017/jog.2021.31.
21. Enderlin, E. M. & Bartholomaus, T. C. Sharp contrasts in observed and modeled crevasse patterns at Greenland’s marine terminating glaciers. *The Cryosphere* **14**, 4121–4133 (2020).
22. van der Veen, C. J. Crevasses on glaciers. *Polar Geography* **23**, 213–245 (1999).
23. Campbell, S. *et al.* Strain-rate estimates for crevasse formation at an alpine ice divide: Mount Hunter, Alaska. *Annals of Glaciology* **54**, 200–208 (2013).
24. Mottram, R. H. & Benn, D. I. Testing crevasse-depth models: a field study at Breiðamerkurjökull, Iceland. *Journal of Glaciology* **55**, 746–752 (2009).
25. Albrecht, T. & Levermann, A. Fracture field for large-scale ice dynamics. *Journal of Glaciology* **58**, 165–176 (2012).
26. Clason, C. C. *et al.* Modelling the transfer of supraglacial meltwater to the bed of Leverett Glacier, Southwest Greenland. *The Cryosphere* **9**, 123–138 (2015).
27. Izeboud, M. & Lhermitte, S. Damage detection on antarctic ice shelves using the normalised radon transform. *Remote Sensing of Environment* **284**, 113359 (2023).
28. Van Wyk de Vries, M., Lea, J. M. & Ashmore, D. W. Crevasse density, orientation and temporal variability at Narsap Sermia, Greenland. *Journal of Glaciology* 1–13 (2023) doi:10.1017/jog.2023.3.
29. Lai, C.-Y. *et al.* Vulnerability of Antarctica’s ice shelves to meltwater-driven fracture. *Nature* **584**, 574–578 (2020).
30. Surawy-Stepney, T., Hogg, A. E., Cornford, S. L. & Hogg, D. C. Mapping Antarctic crevasses and their evolution with deep learning applied to satellite radar imagery. *The Cryosphere* **17**, 4421–4445 (2023).
31. Porter, C. *et al.* ArcticDEM - Strips, Version 4.1. Harvard Dataverse <https://doi.org/10.7910/DVN/C98DVS> (2022).
32. Khazendar, A. *et al.* Interruption of two decades of Jakobshavn Isbrae acceleration and thinning as regional ocean cools. *Nat. Geosci.* **12**, 277–283 (2019).
33. Parizek, B. R. *et al.* Ice-cliff failure via retrogressive slumping. *Geology* **47**, 449–452 (2019).

34. Howat, I. M., Joughin, I. & Scambos, T. A. Rapid Changes in Ice Discharge from Greenland Outlet Glaciers. *Science* **315**, 1559–1561 (2007).
- 345 35. Moon, T., Joughin, I., Smith, B. & Howat, I. 21st-century evolution of Greenland outlet glacier velocities. *Science* **336**, 576–578 (2012).
36. Reeh, N. Greenland Ice Shelves and Ice Tongues. in *Arctic Ice Shelves and Ice Islands* (eds. Copland, L. & Mueller, D.) 75–106 (Springer Netherlands, Dordrecht, 2017). doi:10.1007/978-94-024-1101-0_4.
- 350 37. Colgan, W. *et al.* Glacier crevasses: Observations, models, and mass balance implications. *Reviews of Geophysics* **54**, 119–161 (2016).
38. van der Veen, C. J. Fracture mechanics approach to penetration of surface crevasses on glaciers. *Cold Regions Science and Technology* **27**, 31–47 (1998).
39. Mankoff, K. D. *et al.* Greenland Ice Sheet solid ice discharge from 1986 through March 355 2020. *Earth System Science Data* **12**, 1367–1383 (2020).
40. Joughin, I., Shean, D. E., Smith, B. E. & Floricioiu, D. A decade of variability on Jakobshavn Isbræ: ocean temperatures pace speed through influence on mélange rigidity. *The Cryosphere* **14**, 211–227 (2020).
41. Black, T. E. & Joughin, I. Multi-decadal retreat of marine-terminating outlet glaciers in 360 northwest and central-west Greenland. *The Cryosphere* **16**, 807–824 (2022).
42. Liu, J., Enderlin, E., Marshall, H.-P. & Khalil, A. Synchronous retreat of southeast Greenland’s peripheral glaciers. *Geophysical Research Letters* **49**, e2022GL097756 (2022).
43. Wood, M. *et al.* Ocean forcing drives glacier retreat in Greenland. *Science Advances* **7**, 365 eaba7282 (2021).
44. Harper, J. T., Humphrey, N. F. & Pfeffer, W. T. Crevasse patterns and the strain-rate tensor: a high-resolution comparison. *Journal of Glaciology* **44**, 68–76 (1998).
45. Müller, L. *et al.* Surges of Harald Moltke Bræ, north-western Greenland: seasonal modulation and initiation at the terminus. *The Cryosphere* **15**, 3355–3375 (2021).
- 370 46. Moon, T. *et al.* Distinct patterns of seasonal Greenland glacier velocity. *Geophys Res Lett* **41**, 7209–7216 (2014).
47. Vijay, S. *et al.* Greenland ice-sheet wide glacier classification based on two distinct seasonal ice velocity behaviors. *J Glaciol* 1–8 (2021) doi:10.1017/jog.2021.89.
48. Khan, S. A. *et al.* Greenland Mass Trends From Airborne and Satellite Altimetry During 375 2011–2020. *Journal of Geophysical Research: Earth Surface* **127**, e2021JF006505 (2022).
49. Krug, J., Weiss, J., Gagliardini, O. & Durand, G. Combining damage and fracture mechanics to model calving. *The Cryosphere* **8**, 2101–2117 (2014).

Methods

380 **Crevasse Detection**

Crevasse depth detection from ArcticDEM strips

We mapped crevasses using 2-m resolution ArcticDEM v4.1 strips³¹ provided by the Polar Geospatial Center (PGC). The method, which we make public as a Python package and associated Jupyter Notebooks (<https://github.com/trchudley/crevdem>), will also work on
385 other 2 m strips provided by the PGC as part of the REMA⁵⁰ or EarthDEM⁵¹ projects, although we cannot guarantee the optimal length scale we determine here is representative of other sectors of the Cryosphere. We first preprocessed the strips by filtering them only to good-quality ice surfaces. This was done by filtering strips to ‘good’ data as indicated by the PGC-provided bitmasks; filtering out bedrock using the Greenland
390 Ice Mapping Project (GrIMP) Ice and Ocean classification mask⁵²; and geoid-correcting the heights to mean sea level using the EIGEN-6C4 geoid model⁵³ provided within BedMachine v4⁵⁴. Finally, when over 1 km² of strip area is < 10 m above mean sea level (AMSL), we applied a routine to filter out ‘marine surfaces’ (ocean, sea ice, and low-lying ice mélange) following a previously published iceberg detection routine⁵⁵. In this
395 approach, we constructed a histogram of elevation in 0.25 m bins between -15 and +15 m AMSL, and identified contemporaneous sea level as the modal bin. We assigned all regions beneath 10 m of our determined contemporaneous sea level as marine surfaces, leaving only terrestrial ice and floating ice tongues.

400 After pre-processing, we determined the observed open-air crevasse depth, which we define here as the difference between the raw DEM height and a nominal ‘filled crevasse’ surface. We first detrended the DEM using a large Gaussian filter (standard deviation 200 m), before applying a black top hat (BTH) filter to the detrended surface to determine the negative deviation from the local maxima⁵⁶. Gaussian and BTH filters were both applied
405 using OpenCV implementations⁵⁷. The diameter of the BTH kernel was set to be 60 m, following spatial variogram analysis of crevassed surfaces around Greenland (see section ‘Determining the optimal crevasse length scale’). Following previous approaches⁵⁶, we identify pixels as ‘crevassed’ where the BTH-filtered value is greater than a threshold value, here > 1 m. To generate a nominal ‘crevasse-filled’ surface, we further remove the
410 crevassed pixels and filled the surfaces using an inverse-distance weighting algorithm as implemented in GDAL⁵⁸, followed by two 3×3 averaging filter smoothing operations to dampen artefacts. Crevasse depth was determined as the difference between the interpolated ‘surface’ and the crevasse bottom in the raw DEM.

Determining the optimal crevasse length scale

415 To determine the kernel size, we assessed the typical crevasse length scale by modelling
the spatial covariance, or variogram, which quantifies the variance of spatial
measurements as a function of their separation distance ⁵⁹. The variogram was used to
determine the range, or separation distance at which measurements are spatially
uncorrelated. This parameter has previously been used to determine the optimal kernel
420 size for BTH filtering of DEMs ⁵⁶. To find a representative range parameter, we estimated
the ranges at four different glaciers covering a range of sectors and dynamic contexts:
Sermeq Kujalleq (Jakobshavn Isbræ), Sermeq Kujalleq (Store Glacier), KJV Steenstrups
Nordre Bræ, and Isunnguata Sermia. We manually identified five 1500 × 1500 m sample
zones, which we subjectively ranked on an ordinal scale of ‘crevasse intensity’ from 0 (no
425 crevasses) to 4 (most crevassed region of glacier). We then constructed spatial
variograms of the five sample zones using SciKit-GStat ⁶⁰. We use DEMs from 2021
(Supplementary Fig. 2-5), which we detrended as described above, randomly sampling 2%
of the pixels within the sample zone to increase computational efficiency. To estimate the
representative crevasse width, we used the range of the variograms estimated using a
430 Gaussian variogram model, which best fit our experimental variograms. The mean
estimated spatial range of the most crevassed sample regions (crevasse intensity = 4) was
62.4 m; the mean estimated spatial of the top two most crevassed regions (crevasse
intensity ≥ 3) was 57.3 m (Supplementary Fig. 2-5). We selected 60 m as a representative
range (and thus kernel size) to apply to fast-flowing regions of the Greenland Ice Sheet.

435 Ice-sheet wide processing and mosaicking

We produced GrIS-wide maps of crevasses in 2016 and 2021, years when ArcticDEM strip
coverage was high and particularly conducive to comprehensive assessment.
To eliminate extraneous processing in the ice interior, we generously defined an AOI mask
as anywhere melt occurs in the RACMO2.3p2 1 km melt model between 2016 and 2021
440 ⁶¹, dilated by 10 km. We took all strips intersecting this region between April and October
with a reported RMSE < 2 m and a component image baseline < 60 minutes. In total, we
processed 4667 strips in 2016 and 4207 strips in 2021 (Supplementary Table 2), with a
subsequent coverage of our AOI of 75% and 86% respectively (Supplementary Fig. 6). We
note that coverage is biased towards outlet glaciers and no-data regions are commonly
445 high-elevation, low-velocity sectors in the accumulation zone. This benefits our
assessment as no-data regions are largely regions without crevassing present.

Due to the advection of individual crevasses, 2 m resolution crevasse depth maps cannot
be directly compared. Instead, we enabled comparison between 2016 and 2021 by

450 summing crevasse depth maps into 200 m resolution crevasse volume maps, which we refer to as the 'exposed crevasse air volume'. To obtain a single annual mosaic, we found the median value of all overlapping strips where multiple exist. All crevasse volumes discussed in this study have been aggregated into established sectors and basins ⁶². However, for the interested reader, we present samples of changes at select basins at
455 native resolution, alongside contemporaneous changes in the MEaSURES Greenland annual ice sheet velocity mosaics ^{63,64}, in the supplementary material (Supplementary Figs. 7 - 12).

Uncertainty and Method Intercomparison

We assigned a measurement uncertainty to our aggregate crevasse volume
460 measurements by assessing variation in contemporaneous strip measurements. To do this, we assessed variance within the Nioghalvfjerdingsfjorden (79°N) discharge basin in 2021, which we selected due to its high overlapping strip records (up to 21 overlapping strips) and large variation in surface types. Across all valid pixels within the 79°N area of interest, we calculate the per-pixel standard deviation in crevasse depth values across the
465 basin. The mean standard deviation value across the 200 m grid cells was 407 m³ (10,175 m³ km⁻²). We apply this per-pixel uncertainty value to all basins, and present measurement uncertainty as 2 σ error bars within the figures presented in this paper.

As a first-order comparison against alternative crevasse detection methods, we compare our method to contemporaneous crevasse datasets at a previously studied crevasse field
470 (70.5399°, -50.1423°) located at Store Glacier in 2018. Here, there exists UAV-derived 15-cm-resolution map of crevasses (dated 2018-07-08) classified using object-based machine learning techniques ³. We compare this against a Sentinel-2-derived map of crevasses using a Gabor filter approach ²⁸ for the date 2018-07-02, and apply our current approach on an ArcticDEM strip dated 2018-06-24. Data is shown in supplementary figures 13 and
475 14. Overall, there is good agreement between the methods. Individual crevasses are identifiable between the three datasets. In comparison to the Sentinel-2 approach, our method is sensitive to smaller crevasses, as well as less likely to misclassify the edges of snow/ice boundaries. These advantages are balanced by the much higher temporal resolution of the Sentinel-2 stack, which can detect sub-seasonal changes ²⁸. Using the
480 UAV data as ground validation, we assess the limit of crevasse width detectable by our method to be approximately 10 m. This matches the previous assessment made using a more rudimentary ArcticDEM segmentation approach ³.

Limitations

485 The limitations of our dataset are derived from the resolution and optical source data of the raw ArcticDEM strips.

490 First, the 2 m resolution of the source strips places a fundamental lower bound on the minimum identifiable crevasse diameter. In practice, comparison with UAV data has shown that a realistic minimum diameter observable with these methods is ~10 m (see section “Uncertainty and Method Intercomparison”). Although this limits applications for smaller inland crevasses, it is more than sufficient for observation of changes at crevasse fields in fast-flowing (>100 m/a) regions, where the crevasse width averages ~60 m (see section ‘Determining the optimal crevasse length scale’).

495 Second, the reported crevasse depth values produced by our method are commonly in the range of 10-100 m deep. This does not represent full crevasse depth, as even crevasses with surface expressions of only 10s of centimetres have been shown reach depths of hundreds of metres ⁶⁵. However, larger crevasses of the type observed in this study (~10s metres in width) have been observed to be consistently infilled with debris in high-resolution UAV-derived datasets ⁶⁶, limiting the observed depth in optically-derived DEMs. As such, we refer to the volumetric measurements in this study as the ‘exposed crevasse air volume’, acknowledging that full-depth measurements are not possible. Full crevasse depths have extrapolated from simpler 2D profiles in the past ²¹, suggesting that a similar method to extrapolate 3D datasets may be possible in the future.

505 Third, the optical nature of the source data meant that we cannot extract snow-filled crevasses that may be possible to detect using other methods, such as SAR or GPR ⁶⁷. However, the large diameters of crevasses detected here are highly unlikely to fill with snow: in analysis of Sentinel-2 optical imagery with a similar effective resolution for crevasse detection, crevasse density was not observed to change over a seasonal cycle or in an indicative elevation-dependent way that suggested snowfill ²⁸. The month filtering, ablation zone masking, and median mosaicking we performed during the mosaicking process mean we consider it very unlikely that snowfill can explain any of the large-scale multitemporal change we observe in our study. Any small-scale variation should be adequately captured in our uncertainty assessment, alongside other minor sources of measurement variance (e.g. satellite geometry).

515 Fourth, by selecting a relatively shallow BTH threshold of 1 m, we implicitly included features that are not true crevasses (e.g. shallow ditches and river gulleys). We chose to

520 do this as we are interested in volumetric change rather than area change, and these
shallow features do not represent significant contributions to aggregate volume
measurements. Increasing the BTH threshold to a higher value introduces a much larger
volume of false negatives instead of a small volume of false positives. Experimentation
showed that increasing the threshold for crevasse identification may aesthetically improve
525 the binary crevasse mask, but resulted in an increased variance in our volumetric
uncertainty measurements as legitimate crevasses began to be inconsistently masked
from DEM strips. As a result, this means we do not recommend our method for crevasse
area segmentation tasks – other methods have previously been proposed for this task
using ArcticDEM³.

530 Finally, our analysis covers only the years 2016 and 2021, rather than a continuous
dataset over the study period. As a result, there is a chance that changes we detect may
be a result of capturing high interannual variability or measurement error. Due to
limitations of data coverage in the ArcticDEM strip dataset, it is not possible to achieve
535 satisfactory coverage of other years at a Greenland scale. However, we processed
additional years (2017, 2019, and 2020) for the glacier at the head of Anorittup Kangerlua
fjord (Fig. 1), which we present as supplementary figures showing individual mosaics
(Supplementary Fig. 15) and a time-series of aggregate volume (Supplementary Fig. 16).
This additional analysis shows a clear and continuous secular trend in crevasse volume,
540 associated with a parallel increase in glacier velocity (Supplementary Fig. 17). This
supports our inference that significant changes are attributable to real and significant
changes in crevasse volume rather than short-term variability or measurement error.

Discharge

We compared crevasse change to discharge change as a proxy for the bulk dynamic
545 change of ice sectors and basins. This assumes that the time-evolving discharge, ice
velocity, and the magnitude/extent of extensional stress are broadly correlated at a basin
and sectoral scale. Further, as discharge is a function of both ice velocity and outlet size,
comparing bulk crevasse volume to bulk discharge implicitly controlled for available ice
surface area, unlike direct measurements of ice flow velocity or strain rates.

550 Changes in dynamic forcing takes time to propagate through to observed changes in
crevasse fields, as crevasses are the product of opening and closing stresses integrated
over multiple years. As a result, we compared the average annual discharge for the
preceding five years (2012-2016 for the 2016 crevasse dataset and 2017-2021 for the
555 2021 dataset). A period of 5 years was selected to be in line with published estimates of

crevasse lifecycles in studies of valley glaciers^{44,68} and ensured discharge records do not overlap.

We obtained 2012-2021 monthly ice discharge measurements from flux gate
560 measurements at marine-terminating glaciers from two complimentary datasets^{39,69}
(hereafter the 'King' and 'Mankoff' datasets). Each individual dataset covers specific outlet
glaciers, and neither is comprehensive across all Greenland outlets. As the pre-defined
drainage basins⁶² frequently contain multiple outlets, any individual drainage basin may
be comprehensively covered by flux gates from either the King or Mankoff datasets, both,
565 or neither. As a result, we combined the datasets to cover as many discharge basins as
possible. Of the 254 basins in the dataset, we assessed 192 as having discharge records
in at least one dataset. Of these, 185 basins were usable. 138 had outlets
comprehensively covered by both King and Mankoff, so we took the average of the two
datasets. 29 and 16 basins were comprehensively covered only by King or Mankoff
570 respectively. At two basins, unusually, the two datasets covered mutually exclusive outlets
within the basin, and we used the sum of the two datasets to represent full basin
discharge.

Data Availability

Source data (necessary to reproduce this study and the figures within (Greenland-wide
575 crevasse volume rasters, and basin-scale aggregations of crevasse volume and
discharge) have been deposited in a Figshare repository available at
<https://doi.org/10.6084/m9.figshare.23937654> [PRIOR TO PUBLICATION:
<https://figshare.com/s/3085649423185efbe4d0>]. ArcticDEM 2 m strips are available
at <https://doi.org/10.7910/DVN/OHHUKH>. The EIGEN-6C4 model is available as part of
580 the BedMachine v4 at <https://doi.org/10.5067/VLJ5YXKCNGXO>. The GrIMP ice and ocean
classification mask is available at <https://doi.org/10.5067/B8X58MQBFUPA>. Raw Mankoff
discharge data is available at https://doi.org/10.22008/promice/data/ice_discharge.

Code Availability

The full workflow to download and extract crevasses from ArcticDEM and REMA imagery
585 is publicly available as a Python package at <https://github.com/trchudley/crevdem>.

Methods References

50. Howat, I. M. *et al.* The Reference Elevation Model of Antarctica - Strips, Version 4.1. Harvard Dataverse <https://doi.org/10.7910/DVN/X7NDNY> (2022).
51. Porter, C. *et al.* EarthDEM - Strips, Version 1. Harvard Dataverse
590 <https://doi.org/10.7910/DVN/LHE9O7> (2022).
52. Howat, I. M., Negrete, A. & Smith, B. E. The Greenland Ice Mapping Project (GIMP) land classification and surface elevation data sets. *The Cryosphere* **8**, 1509–1518 (2014).
53. Förste, C. *et al.* EIGEN-6C4 The latest combined global gravity field model including
595 GOCE data up to degree and order 2190 of GFZ Potsdam and GRGS Toulouse. 55102156 Bytes, 3 Files GFZ Data Services <https://doi.org/10.5880/ICGEM.2015.1> (2014).
54. Morlighem, M. *et al.* BedMachine v3: Complete Bed Topography and Ocean
600 Bathymetry Mapping of Greenland From Multibeam Echo Sounding Combined With Mass Conservation. *Geophys. Res. Lett.* 2017GL074954 (2017) [doi:10.1002/2017GL074954](https://doi.org/10.1002/2017GL074954).
55. Shiggins, C. J., Lea, J. M. & Brough, S. Automated ArcticDEM iceberg detection tool: insights into area and volume distributions, and their potential application to satellite
605 imagery and modelling of glacier–iceberg–ocean systems. *The Cryosphere* **17**, 15–32 (2023).
56. Kodde, M. P., Pfeifer, N., Gorte, B. G. H., Geist, T. & Höfle, B. Automatic glacier surface analysis from airborne laser scanning. *International Archives of the Photogrammetry, Remote Sensing and Spatial Information Sciences* **36**, 221–226 (2007).
- 610 57. Bradski, G. The OpenCV Library. *Dr. Dobb's Journal: Software Tools for the Professional Programmer* **25**, 120–123 (2000).
58. Rouault, E. *et al.* GDAL. Zenodo <https://doi.org/10.5281/ZENODO.5884351> (2023).
59. Matheron, G. Principles of geostatistics. *Economic Geology* **58**, 1246–1266 (1963).
60. Mälicke, M. SciKit-GStat 1.0: a SciPy-flavored geostatistical variogram estimation
615 toolbox written in Python. *Geoscientific Model Development* **15**, 2505–2532 (2022).
61. Noël, B., van de Berg, W. J., Lhermitte, S. & van den Broeke, M. R. Rapid ablation zone expansion amplifies north Greenland mass loss. *Science Advances* **5**, eaaw0123 (2019).
62. Mouginot, J. & Rignot, E. Glacier catchments/basins for the Greenland Ice Sheet. 4137543 bytes Dryad <https://doi.org/10.7280/D1WT11> (2019).
620

63. Joughin, I. MEaSURES Greenland Ice Velocity Annual Mosaics from SAR and Landsat, Version 5. NASA National Snow and Ice Data Center DAAC <https://doi.org/10.5067/USBL3Z8KF9C3> (2023).
64. Joughin, I., Smith, B. E., Howat, I. M., Scambos, T. & Moon, T. Greenland flow
625 variability from ice-sheet-wide velocity mapping. *Journal of Glaciology* **56**, 415–430 (2010).
65. Hubbard, B. *et al.* Borehole-Based Characterization of Deep Mixed-Mode Crevasses at a Greenlandic Outlet Glacier. *AGU Advances* **2**, e2020AV000291 (2021).
66. Chudley, T. R., Christoffersen, P., Doyle, S. H., Abellan, A. & Snooke, N. High-
630 accuracy UAV photogrammetry of ice sheet dynamics with no ground control. *The Cryosphere* **13**, 955–968 (2019).
67. Thompson, S. S. *et al.* Comparing satellite and helicopter-based methods for observing crevasses, application in East Antarctica. *Cold Regions Science and Technology* **178**, 103128 (2020).
- 635 68. Meier, M. F. The mechanics of crevasse formation. *Internat. Assoc. Scientific Hydrology* **46**, 500–508 (1958).
69. King, M. D. *et al.* Dynamic ice loss from the Greenland Ice Sheet driven by sustained glacier retreat. *Commun Earth Environ* **1**, 1–7 (2020).

Corresponding Author

- 640 Correspondence and requests for materials should be addressed to Tom Chudley, thomas.r.chudley@durham.ac.uk

Acknowledgements

This project was supported by grants from the National Aeronautics and Space Administration (NASA; 80NSSC18K1027 and 80NSSC18M0078) and National Science
645 Foundation Office for Polar Programs (NSF-OPP; A007467501) awarded to IMH. TRC was supported by a Leverhulme Early Career Fellowship (ECF-2022-589). MDK was supported by NASA (80NSSC22K1709). ArcticDEM strips are provided by the Polar Geospatial Center under NSF-OPP awards 1043681, 1559691, and 1542736. We are grateful to Chris Stokes for discussions regarding this paper.

650 Author contributions

TRC: Conceptualisation, methodology, software, formal analysis, investigation, writing – original draft, writing – review & editing, visualisation, funding acquisition.

IMH: Conceptualisation, methodology, writing – review & editing, supervision, project administration, funding acquisition.

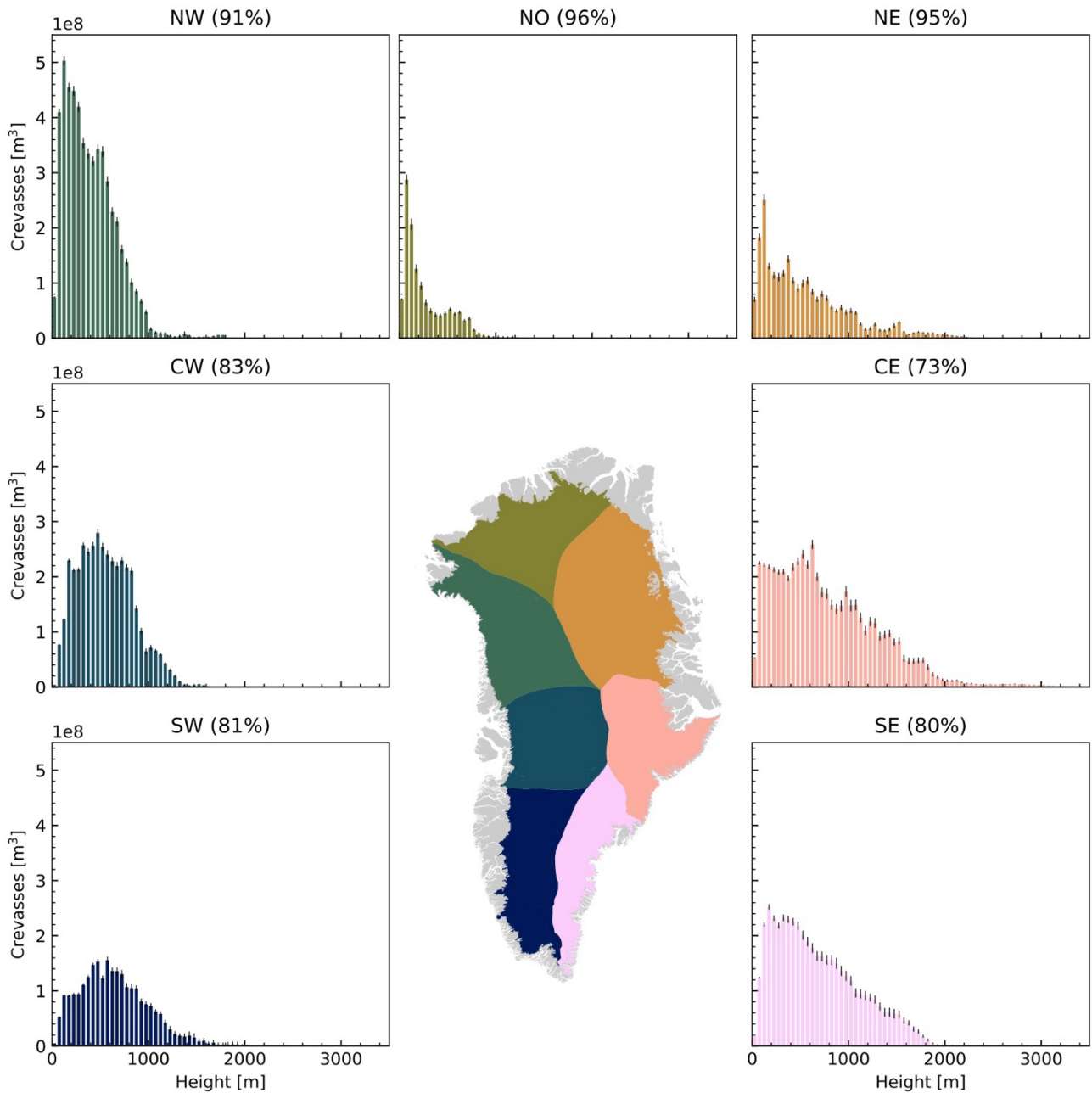
655 **MDK:** Formal analysis, investigation, writing – review and editing.

EJM: Methodology, formal analysis, writing – review & editing.

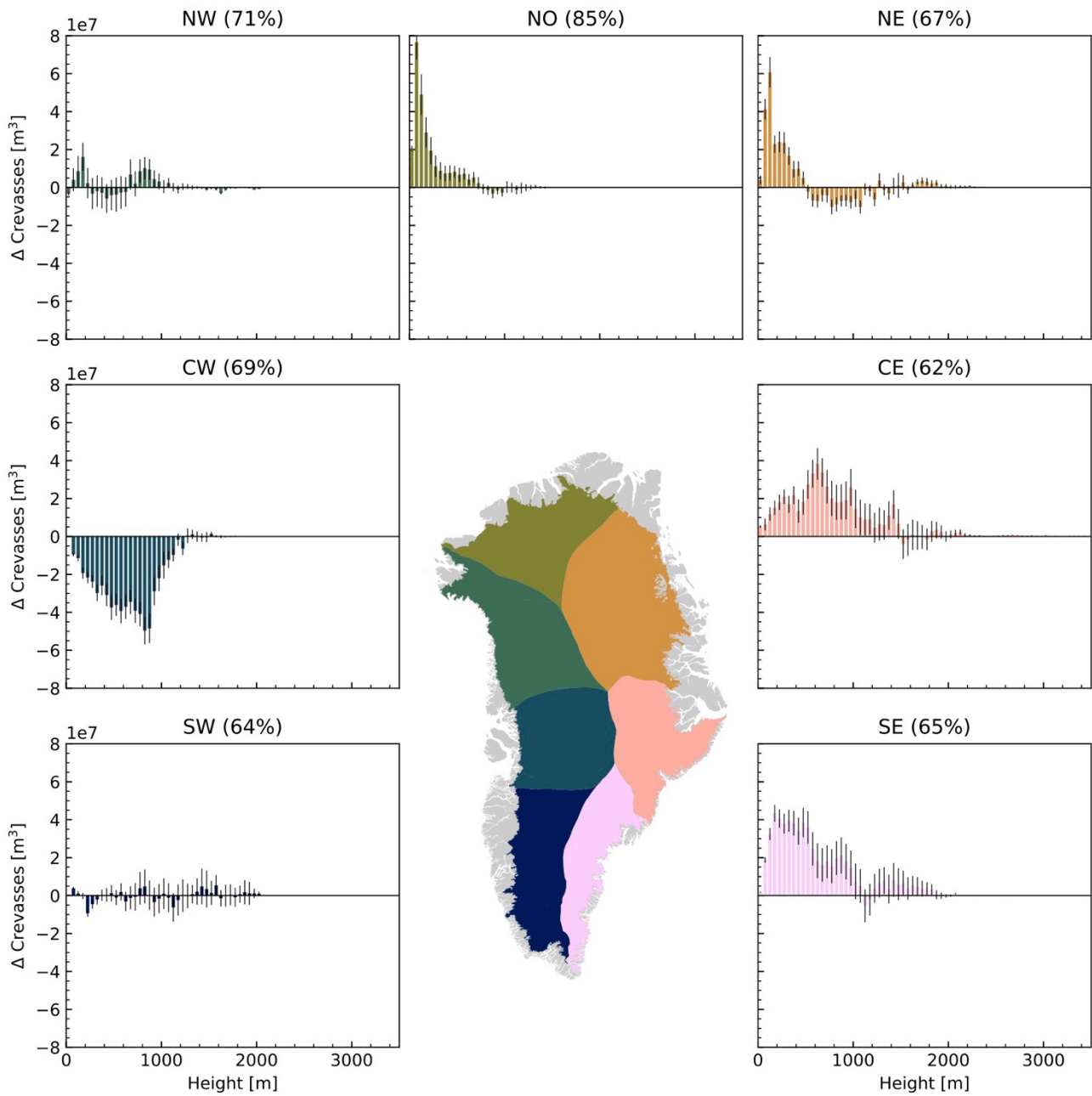
Ethics declaration

The authors declare no competing interests.

660 **Extended Data**



665 **Extended Data Fig. 1: Histograms of sectoral crevasse volume in 2021 by surface elevation.** Error bars represent 2σ uncertainty. Percentages in figure headings represent proportional data coverage of sector.



670 **Extended Data Fig. 2: Histograms of sectoral crevasse volume change between**
2016-2021 by surface elevation. Error bars represent 2σ uncertainty. Percentages in
675 figure headings represent proportional data coverage of sector.

675

Extended Data Table 1: Sectoral and total crevasse volumes for 2021. Discharge represents 2017-2021 average.

680 **Total Sector Area**

Sector	SW	CW	NW	NO	NE	CE	SE	Total
Total Area (km ²)	83825	46784	48140	50103	82405	32150	54442	397849

2021 Coverage

Sector	SW	CW	NW	NO	NE	CE	SE	Total
Percentage Cover	81%	83%	91%	96%	95%	73%	80%	86%
Volume (m ³)	2.52+E09	4.13+E09	5.42+E09	1.28+E09	2.42+E09	5.55+E09	4.66+E09	25.98+E09
Uncertainty (2σ, m ³)	1.92+E08	1.33+E08	1.76+E08	0.97+E08	1.72+E08	2.81+E08	2.53+E08	1.30+E09

685 **2016 Coverage**

Sector	SW	CW	NW	NO	NE	CE	SE	Total
Percentage Cover	81%	81%	76%	86%	67%	69%	68%	75%
Volume (m ³)	2.77+E09	4.54+E09	5.38+E09	1.04+E09	1.82+E09	4.97+E09	3.55+E09	24.06+E09
Uncertainty (2σ, m ³)	2.11+E08	1.32+E08	1.48+E08	0.73+E08	1.14+E08	2.41+E08	2.05+E08	1.12+E09

2016 – 2021 Change

Sector	SW	CW	NW	NO	NE	CE	SE	Total
Percentage Cover	64%	69%	71%	85%	67%	62%	65%	68%

2016 Overlapping Volume (m ³)	2.12+E09	4.43+E09	4.65+E09	1.00+E09	1.79+E09	4.59+E09	3.30+E09	21.89+E09
2016 Uncertainty (2 σ , m ³)	1.53+E08	1.24+E08	1.32+E08	0.71+E08	1.10+E08	2.18+E08	1.95+E08	1.00E+09
2021 Overlapping Volume (m ³)	2.13+E09	3.81+E09	4.70+E09	1.26+E09	1.93+E09	5.11+E09	3.90+E09	22.82+E09
2021 Uncertainty (2 σ , m ³)	1.61+E08	1.17+E08	1.40+E08	0.90+E08	1.19+E08	2.45+E08	2.09+E08	1.09+E09
Difference Volume (m ³)	0.04+E08	-6.30 +E08	0.39+E08	2.53+E08	1.48+E08	5.19+E08	6.00+E08	9.32+E08
Difference Uncertainty (2 σ , m ³)	2.20+E08	1.40+E08	1.58+E08	1.01+E08	1.43+E08	2.81+E08	2.58+E08	13.01+E08
Difference Volume (%)	0.2	-14.2	0.8	25.3	8.3	11.3	18.2	4.3
Difference Uncertainty (%)	10.4	3.2	3.4	10.1	8.0	6.1	7.8	5.9
Significant	N	Y	N	Y	Y	Y	Y	N